PAPER

On the stability and mobility of di-vacancies in tungsten

To cite this article: K. Heinola *et al* 2018 *Nucl. Fusion* **58** 026004

IOP Publishing | International Atomic Energy Agency Nuclear Fusion

Nucl. Fusion **58** (2018) 026004 (8pp) https://doi.org/10.1088/1741-4326/aa99ee

On the stability and mobility of di-vacancies in tungsten

K. Heinola[1], F. Djurabekova[1,2] and T. Ahlgren[1]

EUROfusion Consortium
[1] Department of Physics, University of Helsinki, P.O. Box 64, 00560 Helsinki, Finland
[2] National Research Nuclear University MEPhI, Kashirskoye sh. 31, 115409 Moscow, Russian Federation

E-mail: kalle.heinola@helsinki.fi

Received 22 February 2017, revised 16 October 2017
Accepted for publication 13 November 2017
Published 19 December 2017

Abstract

Properties of small vacancy clusters in tungsten were studied with first-principles calculations. The binding and formation energies of the vacancy clusters increase with the cluster size. Dynamic characteristics of a di-vacancy were specified between room temperature and 700 K with lattice kinetic Monte Carlo calculations, which were parametrised with the present first-principles results for the dissociation barriers. An Arrhenius fit for the di-vacancy diffusion yielded $D = 0.04\exp(-1.65\ \text{eV kT}^{-1})\ \text{cm}^2\ \text{s}^{-1}$, and for the mean lifetime, $\tau = 0.093\exp(1.7\ \text{eV})\ \text{kT}^{-1}$ ps. The di-vacancy system was found to be stable up to 500 K, due to the high energy needed for its dissociation. Having a carbon impurity was found to increase the tungsten di-vacancy binding energy.

Keywords: vacancy clustering, tungsten, di-vacancy, DFT, kinetic Monte Carlo

(Some figures may appear in colour only in the online journal)

1. Introduction

Irradiation-induced defects in solids are the focus of an important study subject in the field of materials science [1]. The formation of large-scale defects, such as voids, cavities and even blistering of the material, is always initiated by the evolution of the immediate primary damage, i.e. the point defects, in the irradiated material. Therefore, understanding of the formation and kinetics of these primary microscopic defects is of fundamental importance, in order to control the observed final defect production. This is considered to be especially vital with materials which are placed to withstand heavy irradiation conditions. In the present work, the material studied is tungsten (W), which has been chosen as a first-wall (FW) material in the incomparable irradiation conditions of the thermonuclear fusion reactor [2–4]. The FW is subjected to abrupt high energy plasma particle bursts during plasma edge localised modes (ELMs). Moreover, a fraction of the irradiation exposure is due to high energy tritium (T) ions from the fusion reactions in the deuterium (D) plasma. However, with D–T plasmas, in addition to the ELMs, the high flux of energetic 14 MeV neutrons from fusion reactions substantially increases radiation damage in FW materials. This ion- and neutron-induced damage worsens the material properties, e.g. by lowering the temperature required for ductile-to-brittle phase change. Moreover, the damaged regions within the FW can result as acting as sinks for the unwanted trapping of fusion fuel T, which in turn is a radiological hazard in next-step fusion devices such as ITER [5].

In the course of irradiation, the ionic and neutron projectiles after penetrating the surface of the target material will interact with the host matrix atoms. The range of these interactions varies depending on the projectile type—neutron-induced damage extends evenly deep in the FW material, whereas ion-induced damage creation is affected by slowing down of the ion due to nuclear and electronic stopping power, making the resulting damage narrower and closer to the FW surface. Depending on the energetics of these interactions due to ions or neutrons, primary damage will be formed in the form of Frenkel pairs, in which the host atoms are kicked out of their lattice sites, leaving a vacant site behind. The number of stable Frenkel pairs created depends mainly on the energy of the incoming particle and the displacement energy of the target material. The vacant sites can already form clusters

during the displacement events or cascades of displacements. The present study focuses on the stability of the small vacancy clusters in body-centered cubic (bcc) W.

The primary vacancy clustering phenomenon in W can still be considered as an unanswered question. The vacancy clustering with different cluster sizes have been observed experimentally [14, 15], but the theoretical explanation is missing. According to recent theoretical first-principles calculations with electron density functional theory (DFT), the initial stage of a vacancy cluster, i.e. the di-vacancy, is unstable or barely stable in pure W [7, 13], leading to speculative conclusions on the formation of larger vacancy clusters. One of the many explanations for making the W di-vacancy stable, and thus allowing formation of larger clusters, is the presence of impurities in the W samples.

In the present research, the stability of small vacancy clusters in W was studied computationally. The main study subjects were the stability and dissociation dynamics of the di-vacancy in pure bulk W, which were scrutinised with DFT and lattice kinetics Monte Carlo (LKMC) calculations, respectively. As a part of the present work, DFT was used for studying the effect of carbon (C) impurity on the di-vacancy stability, since C is typically the most abundant non-metallic intrinsic impurity found in W ($\lesssim$10 μg g^{-1} in high-purity 99.99% poly-crystalline W by Plansee AG).

DFT calculations were performed to determine the energetics of vacancies and the dissociation barriers of a di-vacancy. The barrier heights obtained for pure W were further used in parametrising the dynamical calculations performed using LKMC at temperatures between RT and 700 K. The LKMC and DFT results presented here show the temperature dependence of the di-vacancy dissociation, and the stabilising effect of the carbon impurity.

2. Computational details

2.1. Electron density functional theory

The DFT calculations were performed for determining the ground state energies of the W vacancy systems studied. The Vienna *Ab Initio* Simulation Package (VASP) [16–18] was chosen for this purpose. The electronic ground-state was calculated using the projector-augmented wave (PAW) potentials [19, 20] as provided in VASP. For the volumetric and ionic relaxation the conjugate gradient algorithm was used; the plane wave energy cut-off was 450 eV. The large energy cut-off was used in order to reach high accuracy with every PAW potential used for the elements in this work. No symmetrizations were applied. The electronic and ionic relaxation cut-offs for high-accuracy calculations were chosen as 10^{-5} eV and 10^{-3} eV Å^{-1} respectively. The electron exchange-correlation was described with generalised gradient approximation using Perdew–Burke–Ernzerhof functionals [21, 22]. The six outermost electrons (5*d* and 6*s* sub-shells) of the W atom were used as valence electrons. For the impurity atom C the four (2*s* and 2*p*) outermost electrons were kept in the valence. The partial occupancies were integrated with the Methfessel and Paxton method [23] of the first order. A 3 × 3 × 3 *k*-point mesh was sampled using the Monkhorst and Pack scheme [24]. The convergence obtained with DFT parameters was validated and further checked to reproduce the experimentally obtained properties of W [25, 26]. Supercell with 128 lattice cites was used in the calculations. The present studied systems were mono- (V_1), di- (V_2), tri- (V_3) and four-vacancy (V_4). The V_3 and V_4 were triangular structures as found in [8, 27]. From the relaxed ground states, the corresponding formation and binding energies were determined.

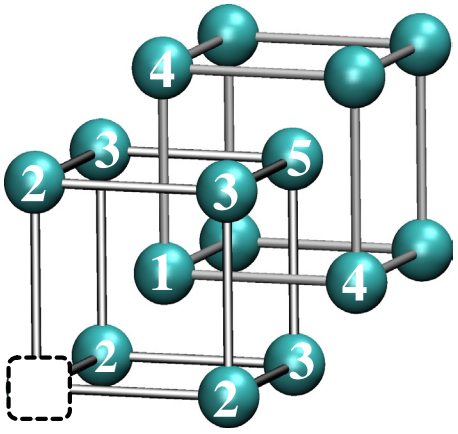

Figure 1. Bcc di-vacancy nearest neighbour configurations used in the DFT and lattice KMC calculations. The five nearest neighbour configurations are numbered with respect to the mono-vacancy denoted with a dotted square.

For the di-vacancy, once the geometry with the lowest energy state was found, the di-vacancy dissociation energetics up to five nearest-neighbour (NN) configurations was determined with the nudged elastic band (NEB) method [28, 29]. The NN positions are presented in figure 1. Seven intermediate images with two endpoint images were used in NEB, to find the geometries giving the minimum energy for the di-vacancy dissociation paths.

Finally, the ground state energies and the resulting dissociation barrier height calculations have been performed by finding their fully relaxed ground states at 0 K. Hence the DFT calculations in this work do not take into account the contribution of the change in the atomistic vibrational entropies ($-T\Delta S_{\mathrm{vib}}$) when compared a defect-free system to a system with vacancies. However, the ΔS_{vib} can be assessed to be small, yielding a significant contribution only at high T. In section 2.2, the need is shown to limit the LKMC calculations to low temperatures, from RT to 700 K, yielding to any change in free energy due to $-T\Delta S_{\mathrm{vib}}$ to be minuscule.

2.2. Lattice kinetic Monte Carlo

The LKMC technique has proven to be an efficient tool in estimating ageing of materials over many years with respect to the thermally activated evolution of extended defects (such as nucleation, growth, annihilation etc), provided that all the activation barriers for the corresponding transitions are available [30–34]. In the present work, the atomistic LKMC approach has been applied in investigating the behaviour of

Table 1. The DFT calculated formation (E_f) and binding (E_b) energies for V_n systems in W with $1 \leqslant n \leqslant 4$. Results are compared with experimental and other DFT results. Units eV.

			DFT			
	Expt.		Other		Present work	
	E_f	E_b	E_f	E_b	E_f	E_b
V_1	3.62 ± 0.2[a]		3.11–3.68[b, c, d, e]		3.33	
V_2 (1NN)		0.7[f]	6.62[c], 7.31[e]	−0.1[g], −0.05[b, h], 0.029[c], 0.05[e]	6.65	0.01
(2NN)				−0.19[c], −0.27[e], −0.39[b]	7.01	−0.35
(3NN)				−0.08[b], −0.12[e]	6.73	−0.07
(4NN)				0[b]	6.64	0.02
(5NN)				−0.13[b]	6.76	−0.10
V_3			9.71[c]	0.04[g], 0.269[c]	9.79	0.19
V_4			12.24[c]	0.64[g], 1.065[c]	12.34	0.78

[a] Reference [6].
[b] Reference [7].
[c] Reference [8].
[d] Reference [9].
[e] Reference [10].
[f] Reference [11].
[g] Reference [12].
[g] Reference [13].

a single di-vacancy cluster in tungsten at different temperatures, assuming the two vacancies are able to come close to one another via the random walk mechanism in a bcc lattice structure. Strictly speaking, the probability of formation of a di-vacancy depends on the concentration of vacancies in tungsten and the diffusion coefficient of a mono-vacancy, but presently we aim to estimate the lifetime and mobility of a di-vacancy after its formation. For this study the LAKIMOCA code [35], which employs the residence time algorithm [36] to assess the migration kinetics of a small cluster within its lifetime, was used. The LAKIMOCA algorithm with the calculation of transition barriers explicitly bound to the initial and final states, however, was modified similarly to the earlier work in [34].

It has previously been shown that the activation barriers rigorously calculated with the account for relaxation effects in the structure, may lead to new insight on the kinematics of the process, which otherwise escapes the sight of a researcher if the relaxation is neglected [32]. The relaxation effect can be obtained either by molecular dynamics simulations applying the appropriate empirical potentials, or by more advanced DFT calculations. For the present study, DFT calculations were used to determine the transition barriers between different states of a di-vacancy, as described in section 2.1. Each state of the di-vacancy was distinguished by the distance between the two vacancies. These were considered to form a cluster while the distance between the vacancies lay in the range from first nearest neighbour (1NN) distance to 5NN. Any vacancies separated by greater distances were considered to represent dissociated di-vacancies.

In the LKMC simulations the tungsten sample was constructed as $20 \times 20 \times 20$ unit cells in the bcc structure, comprising two vacancies. In the LKMC calculations, the probability of di-vacancy formation was not considered. For this reason, the actual size of the cell was not of importance: two vacancies were considered to form a di-vacancy cluster until they were recorded as splitting, i.e. had moved apart to more than 5NN distance; no re-joining events were taken into consideration. The first simulation was performed at RT, and the temperature was increased with an interval of 100 K. The statistics were collected over 200 Monte Carlo trials for each temperature. At 700 K the di-vacancy lifetime became vanishingly small (∼100 ms), and the LKMC were discontinued for higher temperatures.

3. Results

3.1. Di-vacancy energetics with DFT

To validate our DFT results, the properties of bulk W have been calculated and compared with experiments and other DFT calculations found in the literature. The bulk W lattice structures examined were the bcc, fcc and A15 geometries. The results have been published elsewhere [25]. The DFT calculated properties for W mono-vacancy have been presented previously [27, 37]. Our results for the vacancy formation and migration energies agree with the experimental results [6], and with other DFT calculations [9]. In addition, the DFT parameters used have reproduced the reconstruction of the W(1 0 0) surface [26].

The incremental binding energy E_b of a point defect cluster containing $2 \leqslant n \leqslant 4$ defects was calculated with

$$E_b(n) = [E(n-1) + E(1)] - [E(n) + E_0]. \quad (1)$$

$E(n)$ is the total energy of the studied defect system, and $E(n-1)$ is the total energy of one defect dissociated from it. $E(1)$ is the energy of the host lattice with one point defect, and E_0 is the reference energy of perfect bcc W. If the binding energy calculated with equation (1) is positive, the defect system is more stable than the system with one defect separated

Table 2. Binding energies of vacancy-C complexes (eV). Different V_2-impurity dissociation channels shown for the first (1NN) and second (2NN) nearest neighbour V_2 configurations.

AB $\longrightarrow$ A + B	E_b
$V_1C_1 \longrightarrow V_1 + C_1$	2.05
$V_2^{2NN}C_1 \longrightarrow V_1C_1 + V_1$	1.29
$V_2^{2NN}C_1 \longrightarrow V_2^{1NN} + C_1$	3.33
$V_2^{2NN}C_1 \longrightarrow V_2^{2NN} + C_1$	3.69
$V_2^{1NN}C_1 \longrightarrow V_1C_1 + V_1$	0.04
$V_2^{1NN}C_1 \longrightarrow V_2^{1NN} + C_1$	2.08
$V_2^{1NN}C_1 \longrightarrow V_2^{2NN} + C_1$	2.44

from it. The energy needed for a particle to be completely freed from the cluster, i.e. the energy needed for detrapping E_t, is usually defined as the binding energy summed with the migration energy of the fastest particle

$$E_t = E_b + E_m. \quad (2)$$

The migration barrier for W mono-vacancy ($E_m^V = 1.7$ eV) has been presented in figure 2 and in our previous work [27, 37].

The results of the binding energies E_b for the V_n clusters with $2 \leqslant n \leqslant 4$ are presented and compared to other works in table 1. The E_b values agree well with the other theoretical values obtained with DFT [38].

The energetics of the W di-vacancy pose an intriguing question. If two mono-vacancies do not form a di-vacancy system thermodynamically, the agglomeration of vacancies into clusters in pure bulk W is only possible with large mono-vacancy concentrations—where the formation of a tri-vacancy, i.e. simultaneous assimilation of three mono-vacancies, will increase its probability. The only experimental E_b value for the W di-vacancy is 0.7 eV [11]. In an early DFT study, it was stated that the W di-vacancy is unstable even as the two vacancies are separated as far as in the 5NN position [7]. The results showed the 2NN geometry to be the least favorable configuration, with the highest negative E_b. Interestingly, however, the lowest negative E_b was found for the 4NN geometry, and was shown to be nearly null in that work. Numerical values extracted from [7] are shown in table 1. A similar E_b trend for 1NN to 5NN was obtained later by Ventelon *et al* [13], who found 2NN to be the least favourable configuration, with $E_b = -0.46$ eV, and the 4NN geometry to have clearly the lowest negative E_b. DFT work by Kato *et al* [10] yielded E_b values of 0.05, −0.27 and −0.12 eV for the 1NN, 2NN and 3NN di-vacancies, respectively. That work reported the di-vacancy E_b to have a positive value at 1NN, which would allow it to be a thermodynamically stable entity. However, no E_b value for 4NN geometry was reported. More recent DFT results show similar E_b energetics for 1NN and 2NN geometries with 0.007 eV and −0.190 eV [8]. Our results follow the same trend for 1–3NN di-vacancies, with the corresponding E_b values of 0.01, −0.35, −0.07 eV. Further, our E_b results for 4NN and 5NN were found to be 0.02 and −0.10 eV, respectively. Based on this, the most stable di-vacancy configurations in bcc W would be the 1NN and 4NN geometries. The di-vacancy is found to be a semi-stable state, in the sense that

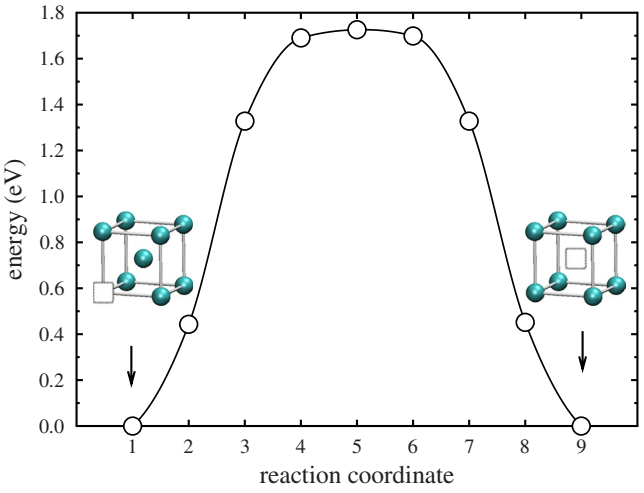

Figure 2. W mono-vacancy migration barrier, as obtained with NEB-DFT.

albeit its E_b for 1NN or 4NN is minuscule, it can still be present as a stable system at a certain temperature range, since the dissociation barrier, i.e. the energy required for detrapping, hinders either of the vacancies to be apart from each other. All the W di-vacancy dissociation barriers as obtained with DFT and NEB are presented in figures 3 and 4. This feature has been also observed and studied recently by Oda *et al*. [39] by using DFT and NEB calculations. From the kinetics point of view, as the temperature increases the effect of the barrier acting as a dissociation limiting step diminishes, and the over-barrier motion becomes thermodynamically more probable.

In [40], it was demonstrated with first-principles calculations that the variations in the bimodal shape of the density of the electronic states (DOS) at the Fermi level (E_F) play a crucial role in the V_1 properties of bcc transition metals. The position of the E_F in the DOS pseudogap contributes to E_f and E_m, and has an effect on the electronic contribution on formation and migration entropies. For the V_2^{1NN} and V_2^{2NN} defect geometries in W, the V_2^{2NN} has been shown to give an increase in the *d*-band local DOS at E_F pseudogap, as compared to the corresponding V_2^{1NN} pseudogap [13]. This result is confirmed in the present work, and the shift in the *d*-band may be attributed to the difference in the geometrical structures of V_2^{1NN} and V_2^{2NN} as follows. The empty lattice site V_1 in bcc W affects the electronic structure of its eight NN atoms, which is seen as variation in their local *d*-bands. The V_2^{2NN} structure influences to its twelve NN W atoms in the [1 0 0] direction. Four out of these twelve W atoms reside on the centre plane (0 1 0) of the V_2^{2NN} geometry, and are joint NN atoms of the two vacancies. As a result, these shared four W atoms are influenced by additional dangling bonds, giving rise to the electronic groundstate of the system. The V_2^{1NN} geometry influences its ten NN W atoms, none of which is shared by the two vacancies. In this case, the electronic system is less distorted (less variance in the local DOS), giving a lower electronic ground state energy. Strong repulsion of V_2^{2NN} in W is a particular feature among bcc transition metals [13], and further investigations are needed to scrutinize the effect of local DOS variation to the stability of the di-vacancies in bcc transition metals. The V_2^{3NN} structure

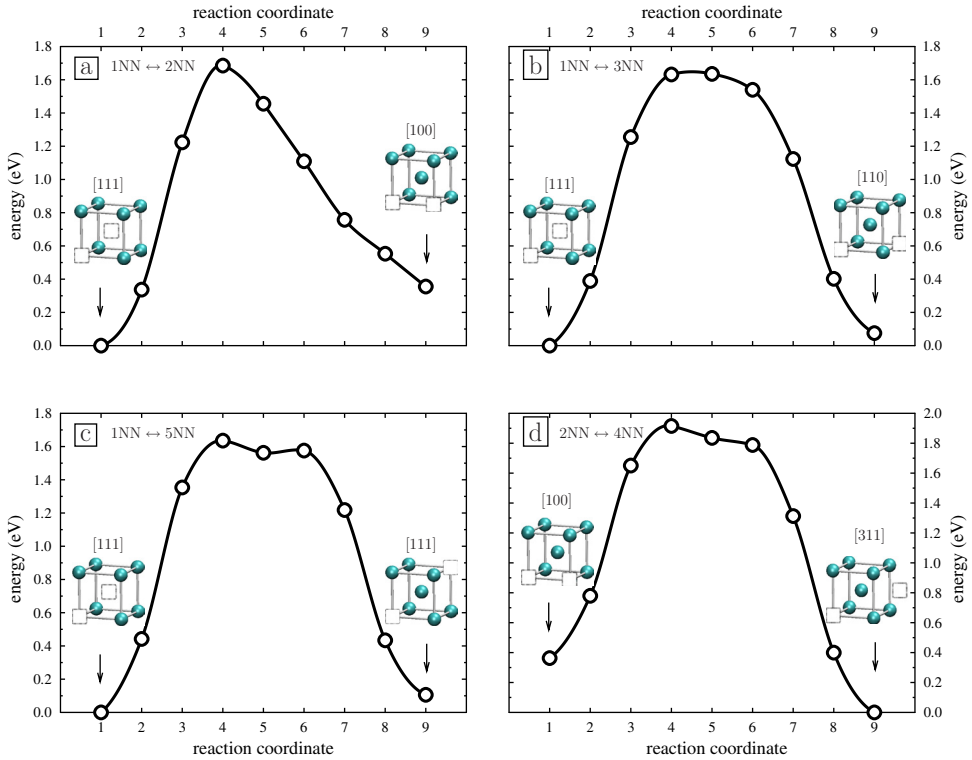

Figure 3. W [1 1 1] (1NN) di-vacancy transition barriers to the neighbouring states (*a*) [1 0 0] (2NN), (*b*) [1 1 0] (3NN) and (*c*) extended [1 1 1] (5NN), as obtained with NEB. Also shown (*d*) the barrier between [1 0 0] (2NN) and [3 1 1] (4NN). Corresponding unit cell geometries of the end points are visualised.

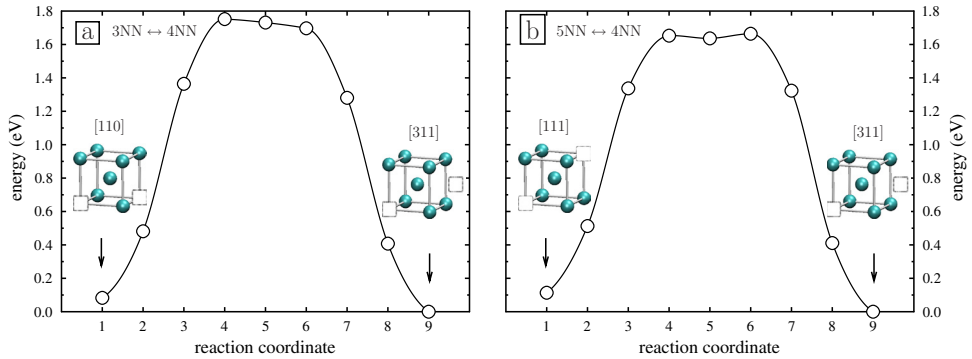

Figure 4. Transition barriers of (*a*) [1 1 0] (3NN) and (*b*) extended [1 1 1] (5NN) di-vacancy to the [3 1 1] (4NN) orientation, as obtained with NEB. Corresponding unit cell geometries of the end points are shown.

has sixteen W NNs, of which two are shared with the vacancies. As a final note, for V_2^{4NN} and V_2^{5NN}, the number of W NNs is sixteen for both structures, but the numbers of shared W NNs are zero and one respectively. There appears to be a correlation with the abovementioned number of shared W atoms for various V_2 geometries and their corresponding E_b values (table 1). Confirming this trend with respect to the effect of local DOS variation in W and other bcc transition metals will be part of a future work.

Figures 3, 4 and 5 present the possible di-vacancy dissociation energetics from 1NN and from 4NN geometries. Once a 1NN geometry is formed, the allowed di-vacancy dissociation pathways found are to 2NN and to 3NN geometries. The formed 4NN structure can dissociate to 2NN, 3NN and 5NN geometries. In figure 5, reported energies for over-barrier motion suggest the 1NN to be a more attractive di-vacancy configuration than the 4NN, since it is energetically more favorable for a mono-vacancy to go back and get trapped to a 1NN than to a 4NN geometry. This result is confirmed with LKMC calculations presented in section 3.2 and figure 7.

Recent work on formation of W di-vacancies has shown that di-vacancies can be stabilised by enriched hydrogen [10]. In that work, the most stable configuration was the 2NN di-vacancy with hydrogen $V_2^{2NN}H_1$. Similar di-vacancy stabilisation effects can be expected with enriched helium, due to its ability to bind strongly with the W mono-vacancy [7, 41]. In the present work, the effect of carbon (C) impurity atoms was examined. It was found that in the presence of C impurity the 2NN di-vacancy becomes more stable than

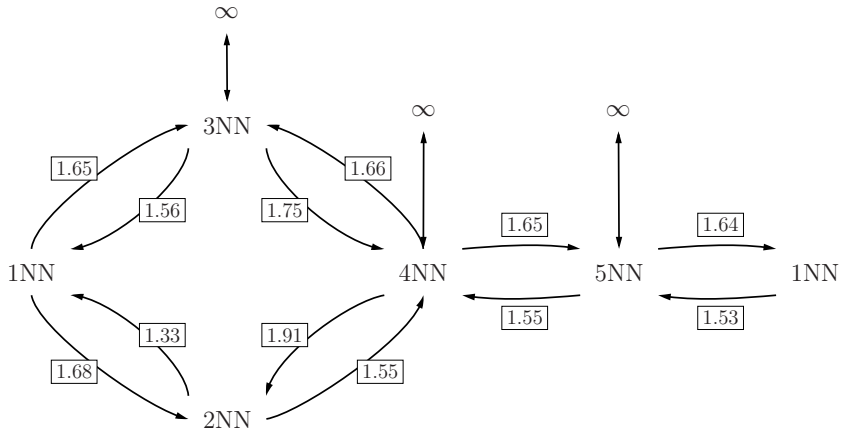

Figure 5. DFT obtained potential barrier heights (boxed values in units of eV) used in the KMC calculations for di-vacancy NN transitions. Barrier to split the di-vacancy, i.e. transition from 3NN, 4NN and 5NN to ∞, was taken as 1.7 eV.

the 1NN di-vacancy: the corresponding E_b for $V_2^{2NN}C_1$ and $V_2^{1NN}C_1$ is 1.29 eV and 0.04 eV (see table 1). The stabilization of the V_2^{2NN} is due to the C residing inbetween the two vacancies, at an octahedral site bonding with the four NN W atoms. These four NN W atoms in the (0 1 0) plane have two dangling bonds each, due to the missing W atoms forming the V_2^{2NN} configuration in the [1 0 0] direction. The electronic groundstate of this system gets stabilized by the add-electrons provided by the C impurity atom located at the abovementioned octahedral site: this is the nearest position with respect to the four W atoms having two dangling bonds, and the C atom shares its valence electrons, thus forming a bond with these host lattice atoms. In the V_2^{1NN} configuration, the surrounding W atoms have only single dangling bonds, and the most stable location for a C impurity was found on the octahedral site in one of the mono-vacancies in the V_2^{1NN} system. Thus, the C atom can be considered to interact only with the V_1 in which it resides, whereas in the V_2^{2NN} configuration the C atom interacts with the whole system, via residing inbetween the two V_1 sites. Interestingly, the DFT E_b result for the $V_2^{1NN}C_1$ configuration suggests, that it is thermodynamically nearly equal in configuration to the V_1C_1 system, with a V_1 far from it (table 2). Further, the E_b for $V_2^{2NN}C_1$ obtained with DFT indicate (table 2), that at high temperatures the 2NN V_2C_1 could dissociate as $V_2^{2NN}C_1 \rightarrow V_1C_1 + V_1$. Taking into account the V_1 migration energy $E_m^{V_1} = 1.7$ eV results in a detrapping energy of ∼3 eV. This leads to the conclusion that the C–di-vacancy system $V_2^{2NN}C_1$ is kinetically stable up to extremely high temperatures.

3.2. Kinematics of W di-vacancy

As described in section 2.2, the stability of the di-vacancy was determined with lattice KMC method using the LAKIMOCA [32]. The mono-vacancy diffuses via jumps to nearest-neighbouring lattice cites in the [111] direction. Thus, a limited number of available cites are for a vacancy to jump to and from the di-vacancy system. Longer jumps in the [1 0 0] direction result in a large potential barrier, which hinders vacancy

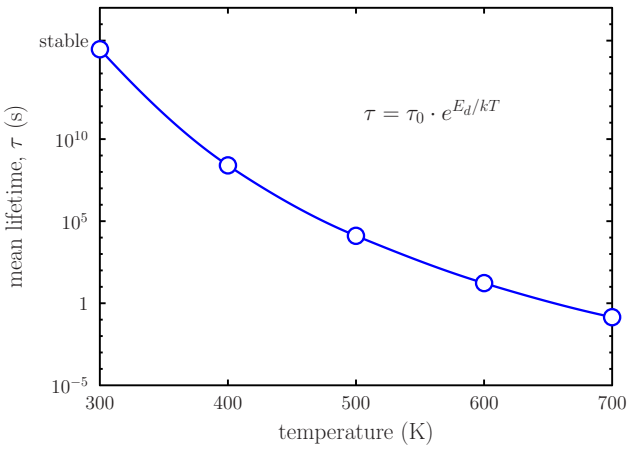

Figure 6. Mean lifetime of the W di-vacancy as function of temperature obtained with lattice KMC calculations. An Arrhenius fit yields $\tau_0 = 0.093 \pm 0.020$ ps and $E_d = 1.70 \pm 0.01$ eV.

motion. For example, a NEB calculation with DFT for 1NN ↔ 4NN transition resulted in a potential barrier of 5 eV, which leads to an energetically highly improbable transition.

The residence time algorithm implemented in the LAKIMOCA code makes it possible to investigate the kinematics of the system evolution, since it assesses the time spent by the system for each transition. Considering the entire population of the non-interacting di-vacancies present in the real system as a unit (corresponding to the KMC simulations of a single di-vacancy with numerous trials), we can plot the KMC result as a distribution of this population between the different states (1NN, 3NN, 4NN and 5NN) as fractions at each time interval.

Figures 3 and 4 present the di-vacancy transition barriers, as obtained with NEB-DFT. The heights of the barriers were used as input in the KMC calculations. The potential barriers for transitions 1NN → 2NN → 4NN → 5NN were found as 1.68 eV, 1.55 eV and 1.65 eV, respectively. For reverse motion 1NN ← 2NN ← 4NN ← 5NN the corresponding barriers were obtained as 1.33 eV, 1.91 eV and 1.55 eV. Transitions 1NN → 3NN → 4NN resulted in 1.65 eV and 1.75 eV (reverse motion 1.56 eV and 1.66 eV) and for 1NN → 5NN the barrier was 1.64 eV (reverse motion 1.53 eV). The di-vacancy was

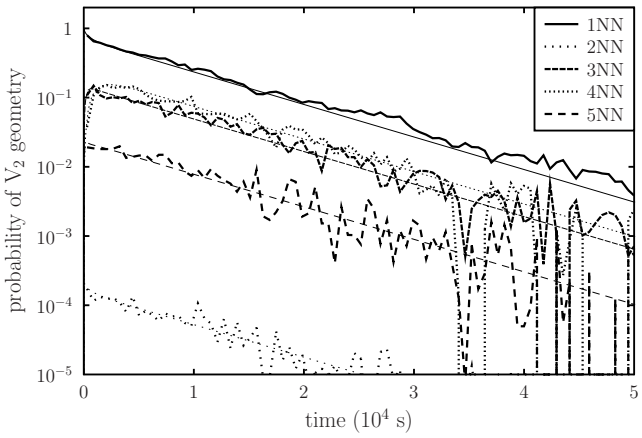

Figure 7. Occupation time of different W di-vacancy geometries at 500 K, as obtained with KMC. The most favourable geometry is the 1NN structure. The 2NN is the most unstable configuration, due to the low transition barriers from 2NN to 1NN and 4NN geometries (see figure 3). Straight lines correspond to the results obtained with Master equations (see text for details).

considered to be split, if the random jump took place beyond 5NN (1.7 eV).

The KMC resulted W di-vacancy diffusion pre-exponential factor and the effective migration barrier are $D_0 = 0.040 \pm 0.006$ cm^2 s^{-1} and $E_m = 1.653 \pm 0.005$ eV respectively. These values are comparable with the experimental values for the W mono-vacancy diffusion (0.04 cm^2 s^{-1} and 1.78 eV by Mundy *et al* [42]). The theoretical value obtained for the mono-vacancy diffusion barrier was 1.7 eV [27].

Figure 6 presents the calculated di-vacancy mean lifetime, τ, as a function of temperature from RT to 700 K. It can be seen, that once a di-vacancy is formed at RT, it will remain as a stable entity with similar diffusion properties as the mono-vacancy. However, the lifetime of the di-vacancy will rapidly decrease as the temperature increases. At 500 K, the lifetime is ∼28 h, while at 700 K it is much less than 1 s.

A detailed KMC analysis was done at temperature 500 K, where the di-vacancies are found to be moderately stable. The fractions of all the states within the time span of the longest lasting di-vacancy were analysed. This time was divided evenly between 100 bins. Every KMC step of the di-vacancy state was analysed and recorded in the bin of the time interval corresponding to the given transition. Every record was weighted by the actual time the transition lasted within the interval. The result of this analysis is presented in figure 7. Here, the KMC simulation results are compared to the Master equations written and solved similarly as in [32]. From the figure 7 results can be seen, that the 1NN di-vacancy configuration is the most stable one, since the di-vacancy spends most of the time in this state. The 4NN and 3NN configurations are the next most stable di-vacancy structures, whereas the 5NN appears less frequently, which may be an indication that a di-vacancy residency structure just before it is being dissociated. The most unstable di-vacancy structure in W is the 2NN geometry. From figure 7 it can be seen that the di-vacancy clearly spends the least time in this geometry, which indicates an unbound state. Once a 2NN structure is formed, the di-vacancy most probably converts back to a 1NN geometry. This can be considered as the di-vacancy diffusion mechanism, if the resulting 1NN is different in lattice orientation from the 1NN preceding the unstable 2NN state: the di-vacancy diffusion can be considered as propagating via a 1NN → 2NN → 1NN mechanism. As a final remark, the clear smooth decreasing tendency of the di-vacancy NN occupation time evolution profiles is defined by the fluctuations in the lifetimes in the different trials.

The KMC simulations result in the conclusion that the formation of a stable W di-vacancy is possible during irradiation events taking place at temperatures ⩽500 K. However, vacancy clustering via diffusion mechanism to large-sized vacancy clusters is unexpected, due to low mono-vacancy-like diffusion pre-exponential factor. As temperatures >500 K, the di-vacancies become exponentially less stable, and the dissociated vacancies may diffuse, and form stable vacancy clusters, such as V_4. Experimental positron annihilation spectroscopy (PAS) analyses [14, 15] in W at 600–750 K have shown the V_1 related PAS intensity signal to decrease or even vanish, giving rise to a signal component indicating the formation of larger vacancy clusters of V_4–V_{10}.

4. Summary and conclusions

To summarise, the properties of small vacancy clusters in bcc W have been studied computationally. DFT and KMC calculations were used in scrutinizing the stability and mobility properties of the di-vacancy. The DFT results indicate the di-vacancy 1NN and 4NN configurations being the most stable geometries. It was found that even when binding energy $E_b \gtrsim 0$ eV, the di-vacancy can still be found as a stable entity, due to the activation energy required for dissociation processes. KMC calculations were done to study the di-vacancy dissociation dynamics in various lattice directions up to 5NN, at temperatures between RT and 700 K. As a result, an effective dissociation barrier was determined, and was found to be $E_d = 1.70$ eV. The di-vacancy diffusion properties were studied accordingly and the effective diffusion parameters found were $D = 0.04 \exp(-1.65 \text{ eV kT}^{-1})$ cm^{-2} s^{-1}. The di-vacancy system has a lifetime of ∼28 h at 500 K. At higher temperatures, the system dissociates rapidly, and the resulting mono-vacancies are allowed to diffuse freely. The C impurity was found to make the 2NN di-vacancy stable. In the presence of impurities, such as H and C, the W di-vacancy can get stabilised even at elevated temperatures, allowing V_n cluster formation.

Acknowledgments

This work has been carried out within the framework of the EUROfusion Consortium and has received funding from the Euratom research and training programme 2014–2018 under grant agreement No 633053. The views and opinions expressed herein do not necessarily reflect those of the European Commission. Grants of computer time from the Center for Scientific Computing (CSC) in Espoo, Finland, and from University of Helsinki, Finland, are gratefully acknowledged.

References

[1] Townsend P., Kelly J. and Hartley N. 1976 *Ion Implantation, Sputtering and Their Applications* (New York: Academic)
[2] ITER Physics Basis Editors *et al* 1999 Chapter 1: Overview and summary *Nucl. Fusion.* **39** 2137
[3] Loarte A. *et al* 2007 Progress in the ITER physics basis chapter 4: power and particle control *Nucl. Fusion.* **47** S203
[4] Rieth M. *et al* 2011 Review on the efda programme on tungsten materials technology and science *J. Nucl. Mater.* **417** 463–7
[5] Taylor N., Alejaldre C. and Cortes P. 2013 *Fusion Sci. Technol.* **64** 111
[6] Rasch K.-D., Siegel R.W. and Schultz H. 1980 Quenching and recovery investigations of vacancies in tungsten *Phil. Mag.* A **41** 91–117
[7] Becquart C. and Domain C. 2007 *Ab initio* calculations about intrinsic point defects and he in w *Nucl. Instr. Meth. Phys. Res.* B **255** 23–6
[8] Muzyk M., Nguyen-Manh D., Kurzydłowski K.J., Baluc N.L. and Dudarev S.L. 2011 Phase stability, point defects, and elastic properties of w-v and w-ta alloys *Phys. Rev.* B **84** 104115
[9] Nguyen-Manh D., Horsfield A.P. and Dudarev S.L. 2006 Self-interstitial atom defects in bcc transition metals: group-specific trends *Phys. Rev.* B **73**
[10] Kato D., Iwakiri H. and Morishita K. 2011 Formation of vacancy clusters in tungsten crystals under hydrogen-rich condition *J. Nucl. Mater.* **417** 1115–8
[11] Park J.Y., Huang H.-C.W., Siegel R.W. and Balluffi R.W. 1983 A quantitative study of vacancy defects in quenched tungsten by combined field-ion microscopy and electrical resistometry *Phil. Mag.* A **48** 397–419
[12] Becquart C., Domain C., Sarkar U., DeBacker A. and Hou M. 2010 Microstructural evolution of irradiated tungsten: *ab initio* parameterisation of an okmc model *J. Nucl. Mater.* **403** 75–88
[13] Ventelon L., Willaime F., Fu C.-C., Heran M. and Ginoux I. 2012 *Ab initio* investigation of radiation defects in tungsten: Structure of self-interstitials and specificity of di-vacancies compared to other bcc transition metals *J. Nucl. Mater.* **425** 16–21
[14] Eleveld H. and van Veen A. 1992 Deuterium interaction with impurities in tungsten studied with tds *J. Nucl. Mater.* **191** 433–8
[15] Eleveld H. and van Veen A. 1994 Void growth and thermal desorption of deuterium from voids in tungsten *J. Nucl. Mater.* **212** 1421–5
[16] Kresse G. and Hafner J. 1993 *Ab initio* molecular dynamics for liquid metals *Phys. Rev.* B **47** 558–61
[17] Kresse G. and Hafner J. 1994 *Ab initio* molecular-dynamics simulation of the liquid-metal-amorphous-semiconductor transition in germanium *Phys. Rev.* B **49** 14251–69
[18] Kresse G. and Furthmüller J. 1996 Efficient iterative schemes for *ab initio* total-energy calculations using a plane-wave basis set *Phys. Rev.* B **54** 11169–86
[19] Blöchl P.E. 1994 Projector augmented-wave method *Phys. Rev.* B **50** 17953–79
[20] Kresse G. and Joubert D. 1999 From ultrasoft pseudopotentials to the projector augmented-wave method *Phys. Rev.* B **59** 1758–75
[21] Perdew J.P., Burke K. and Ernzerhof M. 1996 Generalized gradient approximation made simple *Phys. Rev. Lett.* **77** 3865–8
[22] Zhang Y. and Yang W. 1998 Generalized gradient approximation made simple *Phys. Rev. Lett.* **80** 890
[23] Methfessel M. and Paxton A.T. 1989 High-precision sampling for brillouin-zone integration in metals *Phys. Rev.* B **40** 3616–21
[24] Monkhorst H.J. and Pack J.D. 1976 Special points for brillouin-zone integrations *Phys. Rev.* B **13** 5188–92
[25] Heinola K. and Ahlgren T. 2010 Diffusion of hydrogen in bcc tungsten studied with first principle calculations *J. Appl. Phys.* **107** 113531
[26] Heinola K. and Ahlgren T. 2010 First-principles study of h on the reconstructed w(1 0 0) surface *Phys. Rev.* B **81** 073409
[27] Ahlgren T., Heinola K., Juslin N. and Kuronen A. 2010 Bond-order potential for point and extended defect simulations in tungsten *J. Appl. Phys.* **107** 033516
[28] Mills G., Jonsson H. and Schenter G.K. 1994 Reversible work transition state theory: application to dissociative adsorption of hydrogen *Surf. Sci.* **324** 305–37
[29] Jonsson H., Mills G. and Jacobsen K.W. 1998 *Classical and Quantum Dynamics in Condensed Phase Simulations* (Singapore: World Scientific)
[30] Soneda N. and dela Rubia T.D. 1998 Physics of condensed matter structure defects and mechanical properties *Phil. Mag.* A **78** 995
[31] Caturla M.J., Soneda N., Alonso E., Wirth B.D., de la Rubia T.D. and Perlado J.M. 2000 *J. Nucl. Mater.* **276** 13
[32] Djurabekova F., Malerba L., Pasianot R., Olsson P. and Nordlund K. 2010 Kinetics versus thermodynamics in materials modeling: The case of the di-vacancy in iron *Phil. Mag.* **90** 2585–95
[33] Djurabekova F.G., Domingos R., Cerchiara G., Castin N., Vincent E. and Malerba L. 2007 *Nucl. Instrum. Methods Phys. Res.* B **255** 8
[34] Djurabekova F.G., Malerba L., Domain C. and Becquart C.S. 2007 *Nucl. Instrum. Methods Phys. Res.* B **255** 45
[35] Domain C., Becquart C.S. and Duysen J.-C.V. 1999 *Mater. Res. Soc. Symp. Proc.* 540 643
[36] Bortz A.B., Kalos M.H. and Lebowitz J.L. 1975 *J. Comput. Phys.* **17** 10
[37] Heinola K., Ahlgren T., Nordlund K. and Keinonen J. 2010 Hydrogen interaction with point defects in tungsten *Phys. Rev.* B **82** 094102
[38] Becquart C. and Domain C. 2009 A density functional theory assessment of the clustering behaviour of he and h in tungsten *J. Nucl. Mater.* **386** 109–11
[39] Oda Y., Ito A.M., Takayama A. and Nakamura H. 2014 First-principles study on migrtion of vacancy in tungsten *Plasma Fusion Res.* **9** 3401117
[40] Willaime F., Satta A., Nastar M. and Bacq O.L. 2000 Electronic structure calculations of vacancy parameters in transition metals: impact on the bcc self-diffusion anomaly *Int. J. Quantum Chem.* **77** 927–39
[41] Nguyen-Manh D. and Dudarev S.L. 2015 Trapping of he clusters by inert-gas impurities in tungsten: first-principles predictions and experimental validation *Nucl. Instrum. Methods Phys. Res.* B **352** 86–91
[42] Mundy J.N., Rothman S.J., Lam N.Q., Hoff H.A. and Nowicki L.J. 1978 Self-diffusion in tungsten *Phys. Rev.* B **18** 6566–75